AGU PUBLICATIONS

Geophysical Research Letters

RESEARCH LETTER
10.1002/2015GL063261

Key Points:
- TRMM satellite precipitation signal statistics
- Convective quasi-equilibrium
- Microphysics quasi-equilibrium hypothesis with TRMM and GPM data

Supporting Information:
- Figure S1

Correspondence to:
T. Matsui,
Toshihisa.Matsui-1@nasa.gov

Citation:
Matsui, T., W.-K. Tao, S. J. Munchak, M. Grecu, and G. J. Huffman (2015), Satellite view of quasi-equilibrium states in tropical convection and precipitation microphysics, *Geophys. Res. Lett.*, *42*, 1959–1968, doi:10.1002/2015GL063261.

Received 26 JAN 2015
Accepted 25 FEB 2015
Accepted article online 26 FEB 2015
Published online 27 MAR 2015

Satellite view of quasi-equilibrium states in tropical convection and precipitation microphysics

Toshi Matsui[1,2], Wei-Kuo Tao[1], S. Joseph Munchak[1,2], Mircea Grecu[1,3], and George J. Huffman[1]

[1]Mesoscale Atmospheric Processes Laboratory, NASA Goddard Space Flight Center, Greenbelt, Maryland, USA, [2]Earth System Science Interdisciplinary Center, University of Maryland, College Park, Maryland, USA, [3]GESTAR, Morgan State University, Baltimore, Maryland, USA

Abstract This study shows the time series of statistical composites of precipitation-microphysics signals derived from long-term Tropical Rainfall Measuring Mission (TRMM) satellite observations aggregated over the entire tropical domain (37°N–37°S). The result shows the nearly time-invariant monthly signal statistics throughout this time, confirming convection quasi-equilibrium (CQE) states. Merged precipitation data, with much better temporal and spatial coverage, provide evidence that the equilibrium state occurs on a daily scale. These results further indicate the presence of precipitation microphysics quasi-equilibrium (MQE) within the CQE environment. A simple analytic microphysics framework illustrates the equilibrium precipitation size distribution, as compared with the TRMM radar-based as well as preliminary Global Precipitation Measurement combined retrievals. The MQE readily explains the near-constant tropical precipitation rate, which is roughly balanced with atmospheric radiative cooling rate at the entire tropical scale. Further investigation is required through theoretical, observational, and numerical manners to support the MQE hypothesis.

1. Introduction

Tropical convection and precipitation play significant roles in describing Earth's energy and water budget. A significant element of tropical atmospheric dynamics is explained by the quasi-equilibrium state of radiation-convection adjustment processes, which is a statistical view of weather systems in the tropics [*Emanuel,* 2007]. This is because convective perturbations quickly cascade to gravity waves in tropics, while they are balanced with wind in middle- and high-latitude regions [*Schubert et al.,* 1980]. Thus, robust theoretical development requires a dense network of observations.

Ever since its launch in 1997, the Tropical Rainfall Measuring Mission (TRMM) satellite [*Simpson et al.,* 1988] has been providing the observational cornerstone of tropical precipitation and vertical latent heat structures [*Tao et al.,* 2006]. TRMM has been in space for nearly 18 years and is expected to finish its saga in the middle of 2015, with detailed precipitation measurements being transitioned to the Global Precipitation Measurement (GPM) mission [*Hou et al.,* 2014].

This study provides a macroscopic statistical view of tropical convection, precipitation intensity, and its microphysics state through examining the TRMM-observed direct signals as well as retrieved precipitation products. We will show climatology as well as monthly variations of various TRMM-derived statistical signals in section 2. The time scale of the quasi-equilibrium state of precipitation intensity is discussed in section 3. Then, we demonstrate that additional TRMM signal statistics suggest the presence of precipitation microphysics quasi-equilibrium in section 4. Some potential questions and uncertainties and future directions are discussed in section 5.

2. Quasi-Equilibrium State of TRMM Precipitation Signals

The data used in this study are TRMM Precipitation Radar (PR) attenuation-corrected echo profile (2A25 from *Iguchi et al.* [2000]) and TRMM Microwave Imager 89 GHz brightness temperature (Tb_{85}). Tb_{85} is convolved to the PR footprint with Gaussian weighting [*Matsui et al.,* 2009]; thus sampled within the PR swath width (~250 km with all PR scan angles), whenever PR detects precipitation signals (>20 dB*Z*). These TRMM Level 1B signal data sets are studied from January 2002 to June 2011 over the TRMM-orbit tropical domain (latitude from 37° south to 37° north), which avoids the inconsistency in signal statistics that the orbit boost in mid-2001 introduced.

©2015. American Geophysical Union. All Rights Reserved.

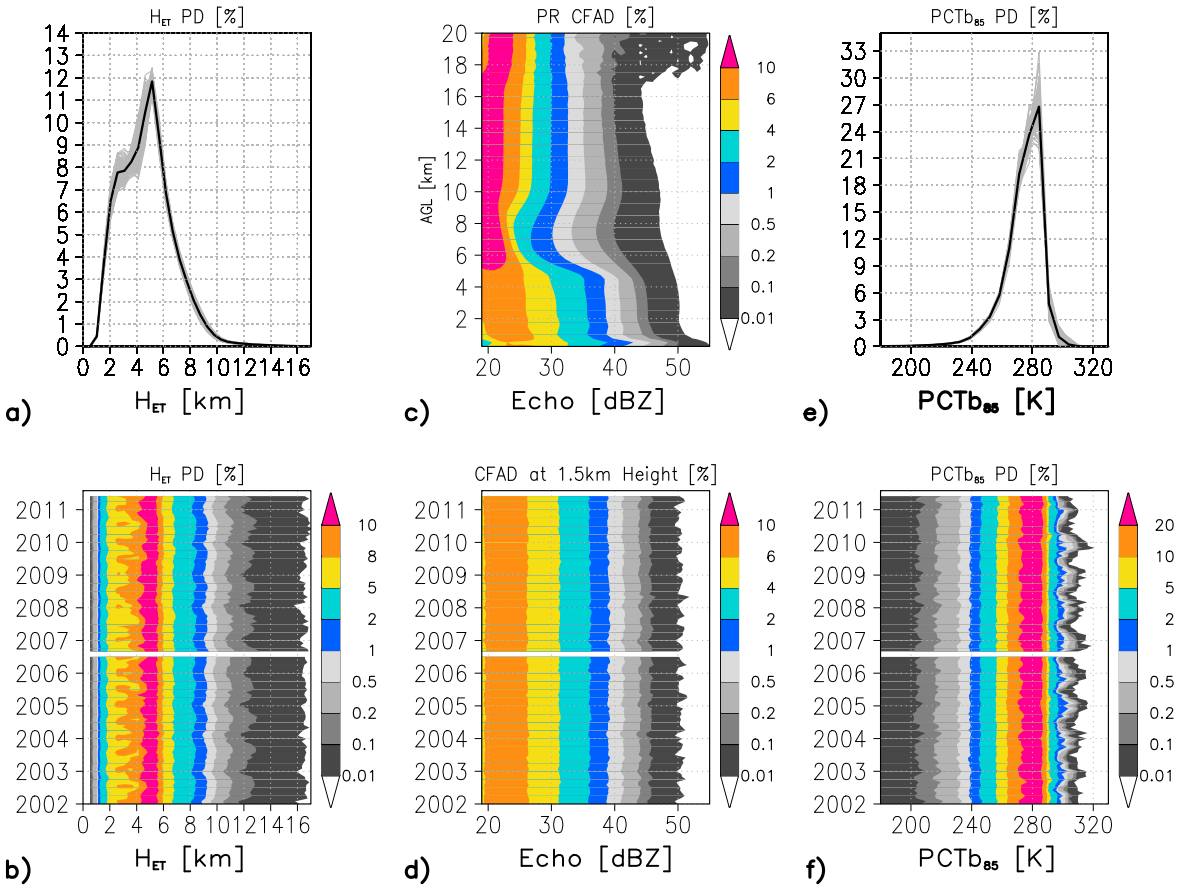

Figure 1. (a) Climatological (thick line) and month-to-month (gray lines) frequencies of PR echo-top height (H_{ET}), (b) time series of monthly frequencies of H_{ET}, (c) climatology of PR Contoured Frequency of Altitude Diagram (CFAD), (d) time series of monthly PR CFADs at 1.5 km above ground level (agl), (e) climatological (thick line) and month-to-month (gray lines) frequencies of PR echo-top height the polarization-corrected microwave brightness temperature at 85 GHz ($PCTb_{85}$), and (f) time series of monthly frequencies of $PCTb_{85}$.

PR echo-top height (H_{ET}) is derived, if the radar echo profile with 250 m vertical sample has values greater than 20 dBZ in three successive layers from the top of atmosphere (TOA). Physically, H_{ET} represents storm height so that higher (smaller) H_{ET} represent deeper (shallower) moist convection. Figure 1a shows the frequencies of H_{ET} over sampling period. A black line shows the climatological frequency, while gray lines show the month-to-month variability from TRMM PR. The frequency peaks at 5.25 km for H_{ET}, and a secondary peak appears at 2.5 km. For H_{ET} greater than 5.25 km, month-to-month variability is remarkably small, while there is relatively large variability for H_{ET} in the range from 2 km to 5.25 km above ground level (agl). However, month-to-month variations are quite small overall, comparing with climatology.

Figure 1b shows the detailed time series of H_{ET} frequencies, and showing biseasonal peak of frequencies of the small-range (~3 km) H_{ET}, contributed by shallow precipitation. Peaks are most likely to appear in January and June, which could be further correlated with the atmospheric radiative cooling rate (section 4). On the other hand, midrange H_{ET} (5–8 km) shows small temporal variability, while the deepest convective echoes (<1%: dark shade) show weak sinusoidal patterns associated with the seasonal cycle due to continental deep convection in boreal summer.

Figure 1c shows the climatology of PR Contoured Frequency of Altitude Diagram (CFAD), which normalizes the histogram of PR echo for each 250 m level. PR echo physically represents the sixth moments of the precipitation particle size and effective density; thus, larger echo is associated with large raindrops and more intense precipitation. Three phases of precipitation particles are deduced from the CFAD structure. An upper layer (10–20 km height) is dominated by solid precipitation processes, which generally result in large ice

©2015. American Geophysical Union. All Rights Reserved.

crystals and relatively small snow aggregate in narrow bins (>1%, color shade), and large graupel and hail particles in the tails (<1%, gray shade) of the distributions.

A middle layer (5–10 km) is dominated by mixed-phase precipitation processes, where ice crystal aggregation and melting result in large increases of PR echo toward this layer at 4–5 km above ground level (agl). Echo modes decrease in this level compared to the levels above 10 km. This is because a significantly large population of deep stratiform precipitation with H_{ET} less than 10 km narrows the echo frequencies, while the echo distribution above 10 km is mainly due to rarely occurred undiluted deep convective precipitation (or hot towers) [*Zipser,* 2003], in which large rimed particles increase the PR echo value significantly. The lower layer (0–5 km) is dominated by liquid-phase precipitation processes, where raindrops create the distributions of PR echo.

Since the sharp increase of the PR echo below 1 km agl is most likely due to surface clutter, we diagnosed a time series of the PR CFAD at 1.5 km agl to investigate near-surface precipitation microphysics. Figure 1d shows the time series of monthly PR frequency at 1.5 km agl. It shows the remarkably similar echo distributions for different months and years. This suggests that near-surface precipitation microphysics is distributed nearly identically over time with very small seasonal and interannual variation.

Figure 1e shows climatological (black line) and month-to-month (gray lines) frequencies of the polarization-corrected Tb_{85} [$PCTb_{85} = Tb_{85V} + c\,(Tb_{85H} - Tb_{85V})$], where Tb_{85H} and Tb_{85V} are horizontal and vertical polarized microwave brightness temperature, respectively; and c is coefficient (0.8 was applied to mask out surface signals by water vapor absorption for most of tropical atmosphere [*Matsui et al.,* 2009]). Depression of $PCTb_{85}$ is physically associated with path-integrated amount of precipitating ice particles, but in comparison to PR dBZ, $PCTb_{85}$ is more sensitive to smaller ice particles due to its shorter (millimeter) wavelength [*Matsui et al.,* 2009]. Note that $PCTb_{85}$ is sampled only if PR-detected precipitation signals.

A peak of the $PCTb_{85}$ frequencies appears to be around 280 K, and distributions are weakly skewed into higher temperature. Large month-to-month temporal variation appears around 270 K. Similar to the H_{ET} case, this is likely due to shallow precipitation. On the other hand, $PCTb_{85}$ less than 270 K shows time-invariant distributions for different months and seasons. The exception is the highest $PCTb_{85}$ (>290 K), showing seasonal variation, probably due to the seasonal dependence of skin temperature over desert regions. There is also very weak seasonality in $PCTb_{85}$ colder than 240 K. The overall structure of frequencies suggests that amount of precipitating ice (represented by $PCTb_{85}$) is distributed nearly identically over time with very small seasonal and interannual variation.

3. Quasi-Equilibrium State of Tropical Precipitation Intensity

The previous section provides the macroscopic view of convective quasi-equilibrium (CQE) state as originally proposed by *Arakawa and Schubert* [1974]. CQE essentially assumes that kinetic energy of the cumulus ensemble is in statistical equilibrium with large-scale forcing. The CQE assumption is typically used for the scale of ~200 km^2 (or even less) for convective parameterization of general circulation models. Consequently, it lacks robustness due to lack of sufficient sampling [*Yano and Plant,* 2012]. On the other hand, TRMM PR observations cover nearly 15 times the entire tropical area in each month. This huge sampling provides the approximately 6.6 million precipitating columns per month to provide the robust CQE statistics.

The detailed structure of CQE is strongly tied with cloud microphysics, since it controls cloud-radiative heating, precipitation efficiency, and latent heat with cloud dynamics [*Grabowski,* 2003]. To clarify the relationships among the radar echo, precipitation rate, and microphysics assumptions, we start from the simple, classical Marshal-Palmer particle size distribution (hereafter MP-PSD).

$$N(D) = N_o \exp[-\Lambda D], \tag{1}$$

where $N(D)$ is particle number density (mm^{-1} m^{-3}) for a given particle diameter (D) (mm); N_o is a constant intercept ($= 8 \times 10^3$ mm^{-1} m^{-3}); Λ is a slope parameter (mm^{-1}) as a function of rainfall rate ($\Lambda = 4.1R^{-0.21}$), which is also associated with the inverse of mean particle diameter. The MP-PSD was established upon observations and states that the precipitation PSD (slope parameter) is well described by precipitation intensity with a constant intercept [*Marshall and Palmer,* 1948]. The terminal velocity of a precipitation particle is typically given by the power law relationship,

$$V_t(D) = \alpha D^{\beta}, \tag{2}$$

©2015. American Geophysical Union. All Rights Reserved.

where α and β are fitted coefficients. *Uijlenhoet* [2001] found α and β must be 3.25 and 0.762 for satisfying the mathematical consistency in MP-PSD. Then total precipitation rate (R) is given by

$$R = \int \rho_l \frac{\pi}{6} D^3 V_t(D) N(D) \ \mathrm{d}D = \rho_l \frac{\pi}{6} \alpha \Gamma(4+\beta) N_o \Lambda^{-(4+\beta)}, \tag{3}$$

where ρ_l is liquid density (= 1.0 g cm^{-3}) and Γ is gamma function. Equation (3) clearly depicts the impact of these PSD and terminal velocity coefficients on the total precipitation rate.

Radar reflectivity is defined as the sixth moment of PSD through the Rayleigh approximation and also expressed by well-known *Z-R* relationship.

$$Z = \int D^6 N(D) \mathrm{d}D = aR^b, \tag{4}$$

where

$$a = \Gamma(7) \left[\frac{\pi}{6} \alpha \Gamma(4+\beta) \right]^{\frac{-7}{4+\beta}} N_o^{\frac{-(3-\beta)}{4+\beta}} \tag{5}$$

$$b = \frac{7}{4+\beta}, \tag{6}$$

where coefficients a and b are 296 and 1.47, respectively, for MP-PSD assumption [*Uijlenhoet,* 2001]. Equations (5) and (6) suggest that the *Z-R* relationship is strongly affected by the assumptions of PSDs and terminal velocity coefficients, too.

Precipitation intensity frequency can be derived from climatological frequency of the PR echo (*pd(Z)*) from Figure 1d, and radar echo is converted into precipitation rate by inverting equation (5). The precipitation intensity frequency shows the exponential decay of precipitation intensity toward heavy precipitation events. PR-MP-PSD estimation shows the physical limit of detecting precipitation at around 0.5 mm h^{-1} (equivalent to ~20 dB*Z*) so that lighter precipitation rate below this threshold cannot be captured due to the PR instrument's limitation.

As noted before, the number of monthly TRMM PR observations is roughly 6.6 million. Although this provides a large sample of convection, it is still a small fraction of the total convection and precipitation cells over the month for the tropics. Thus, we assume that the structure of precipitation intensity frequency should be similar on a fine temporal scale for observations covering a wider area than the narrow PR swath. For this, we also derived the precipitation intensity frequency from TRMM 3B42 data over the same time period to understand the time scale of equilibrium adjustment.

TRMM 3B42 provides more spatially and temporally complete precipitation data, blending microwave and infrared satellite estimates of precipitation, as well as monthly analysis of precipitation gauge data, mostly over land. TRMM 3B42 data sets provide 3-hourly 0.25°-grid precipitation estimates [*Huffman et al.,* 2007, 2010]. With this, we derive climatological precipitation intensity frequency from 3B42 (Figure 2a).

In comparison with the MP-PSD-based PR estimation, 3B42 can capture the distribution of light precipitation well. This is not surprising, because (i) microwave and infrared retrievals better estimate light precipitation in 3B42 data; and (ii) PR footprint size is 5 km, while 3B42 has a quarter degree grid, which tends to include nonprecipitation area in sampling volume, i.e., lowering instantaneous grid-scale precipitation rate.

We have created time series of the intensity frequencies for 3B42 during this time span by averaging for different intervals (14 days, 7 days, and 1 day) to investigate equilibrium adjustment time (Figure 2b). The 14 day composite shows nearly identical precipitation intensity distributions throughout the time period. Comparing three averaging intervals, the time series of 1 day averaging is slightly noisier than 7 day, which is noisier than the 14 day composite; however, structures appears to be very similar between each other.

Overall, the results confirm the robustness of CQE in the view of quasi-equilibrium state of precipitation intensity distribution, which could be established down to at least a 1 day time period. This result also suggests that the monthly statistical equilibrium states of H_{ET}, radar echo, and PCTb$_{85}$ shown in Figure 1 should be expected in the same short time period, if these quantities were sampled much more frequently and over the entire tropical domain.

©2015. American Geophysical Union. All Rights Reserved.

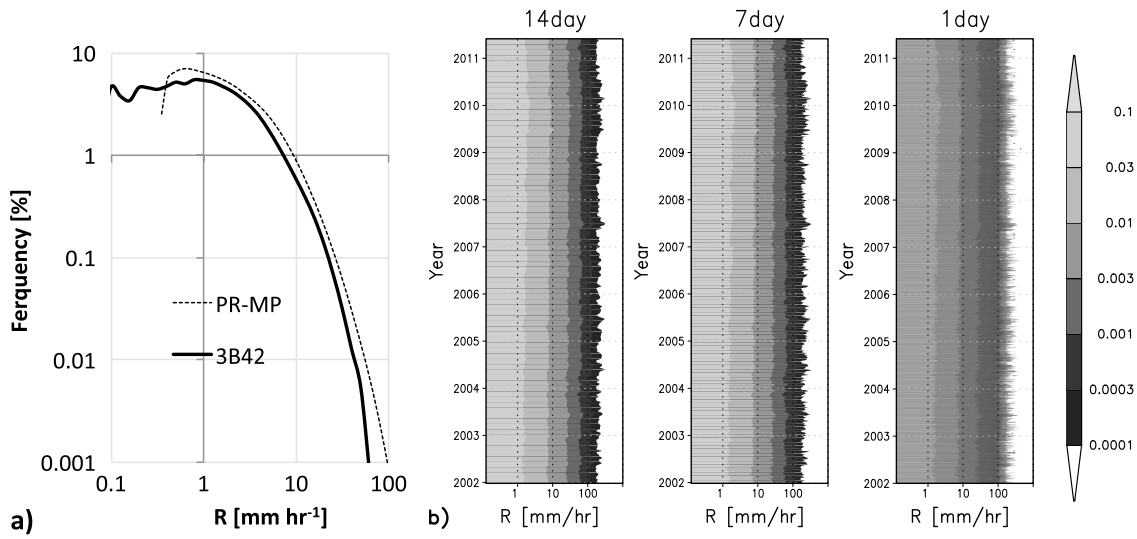

Figure 2. (a) Precipitation intensity frequencies derived from climatological PR echo frequency under assumptions of MP-PSD as well as climatology from TRMM 3B42. (b) Time series of precipitation intensity frequencies composite in 14 day, 7 day, and 1 day periods, using 3B42 product.

4. Hypothesis of Microphysics Quasi-Equilibrium

Precipitation microphysics processes and states are usually associated with convection intensity, characterized by storm height and width for a given thermodynamics state, mesoscale dynamics, and large-scale circulation [*Munchak et al.,* 2012]. The structure of radar composites statistically suggests the microphysics state and process. To explain this, Figures 3a, 3c, and 3d shows H_{ET}-decomposed PR CFAD climatology for shallow ($H_{ET} < 4$ km), middle (4 km $< H_{ET} <$ 7 km), and deep ($H_{ET} > 7$ km) categories.

The shallow category shows narrow distributions of PR echo, and echo distributions become broader toward the surface (2–4 km level), suggesting the raindrop growth process through collision-coalescence and accretion processes. Below 2 km agl, echo growth rate becomes rather limited. The middle category shows the signals of mixed-phase precipitation microphysics processes; above 5 km, the linear increase of radar echo distributions with decreasing altitude suggests the presence of snow aggregation, and this increase suddenly stops at 5 km level due to melting. A slight increase of echo distributions below 5 km is attributed to raindrop growth similar to shallow category. But in comparison with shallow, the growth rate for middle is rather limited, suggesting that raindrop breakup processes start regulating the particle sizes.

The deep category CFAD is somewhat close to total CFAD in Figure 1c, but by removing shallow and middle classes, echo distributions below 5 km are much more widely distributed with ~35 dB*Z* of mode echo. As explained in section 3, the CFAD structure shows distinct solid-, mixed-, and liquid-phase microphysics. Again, the radar echo represents integrated sixth moments of the PSD (equation (4)), so the radar echo is most affected by larger droplets within the radar sampling volume, and the PR CFAD represents statistical distributions of bulk precipitation particle size (and effective density as well for ice-phase particles).

As briefly introduced in section 2, the H_{ET}-classified CFAD structures repeatedly show nearly identical distributions over different months and years. Figures 3b, 3d, and 3f show root-mean-square errors (RMSE) of CFADs by comparing monthly CFADs and climatology CFADs over the 10 year period. Thus, RMSEs indicate the degree of monthly variability in equilibrium distributions of precipitation particle size at each level. Three RMSEs of CFADs show mostly below 0.1% (gray scale), and some small fractions up to 0.5% around the 20 dB*Z* bin, meaning a very small difference between monthly and climatology. Only above 16 km level of deep category CFADs is the RMSE up to 10%. This is due to the limited sample size from continental undiluted hot towers [*Zipser,* 2003].

Overall, these nearly time-invariant patterns of CFADs motivate the following hypothesis.

Tropical precipitation microphysics is in a quasi-equilibrium state.

©2015. American Geophysical Union. All Rights Reserved.

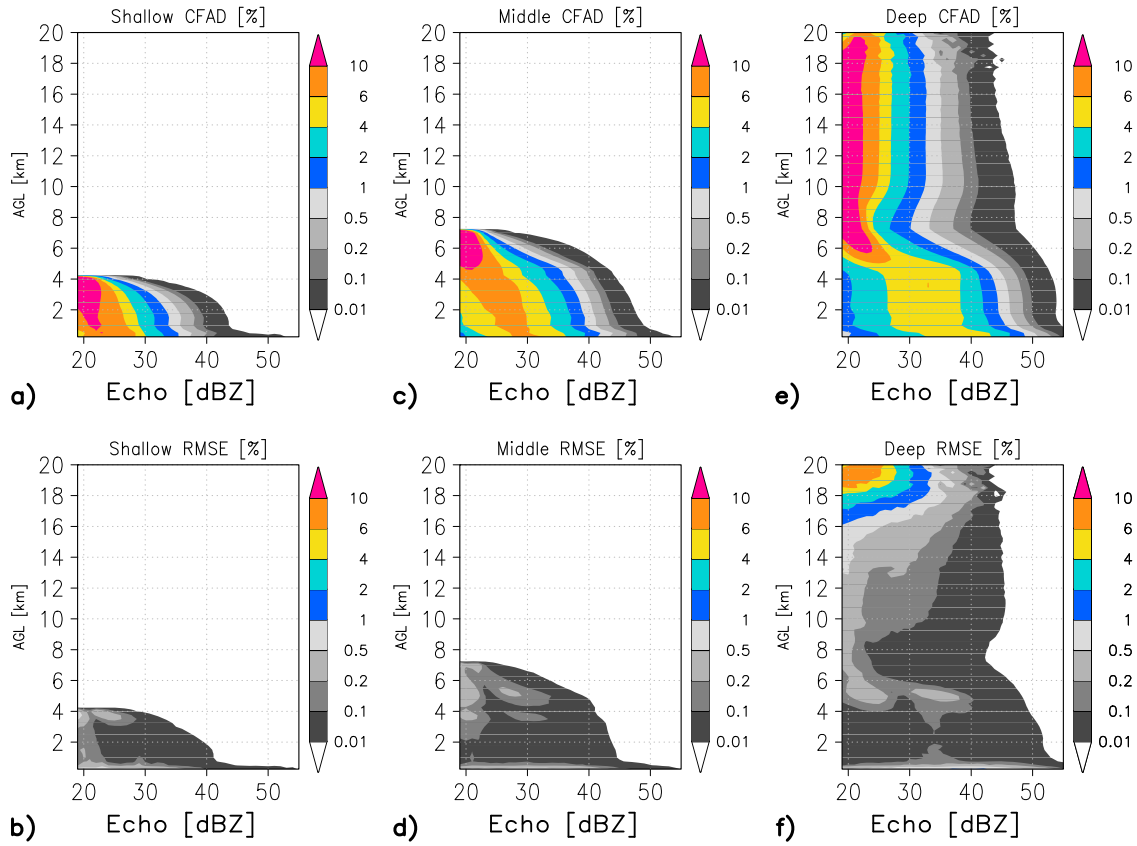

Figure 3. (a) Climatological PR CFADs for shallow category ($H_{ET} < 4$ km), (b) root-mean-square error (RMSE) of CFADs in comparison between month-to-month and climatological CFADs for shallow category, (c) climatological CFAD for middle category (4 km $< H_{ET} <$ 7 km), (d) RMSE of CFADS for middle category, (e) climatological CFAD for deep category (7 km $< H_{ET}$), (f) RMSE of CFADS for deep category.

Similar to the CQE, this should be quasi-equilibrium, hereafter denoted as microphysics quasi-equilibrium (MQE), since there is no true equilibrium state, as seen from the TRMM signal statistics, which shows very small seasonal oscillatory behavior.

To simply illustrate the tropical equilibrium precipitation PSD at the near-surface level, we combine MP-PSD with the TRMM climatology echo distribution derived in Figure 1c. First, PSD is written as a function of size (D) and radar reflectivity (Z) by combining equations (1) and (4);

$$N(D,Z) = N_o \exp\left[-4.1\left(\frac{Z}{a}\right)^{0.12/b} D\right]. \tag{7}$$

Then, we combine equation (7) with equilibrium PR echo frequency climatology ($pd(Z)$, Figure 1c), to estimate equilibrium PSD.

$$N(D)|_{\text{tropics}} = \int N(D,Z)\, pd(Z) \mathrm{d}Z \tag{8}$$

Figure 4a shows MP-PSD-assumed tropical equilibrium PSD (thick black line) from TRMM PR echo climatology. The estimated equilibrium PSDs are more broadly distributed than the reference MP-PSD with 30 dBZ echo (gray line). We found that the equilibrium PSDs can be well ($R^2 = 0.99$) expressed by the second-order polynomial fitting of exponential PSD ($N(D)|_{\text{tropics}} = N_o \exp[c_1 D^2 - c_2 D]$), where c_1 and c_2 are 0.1248 and -3.5633, respectively.

Since the example of MP-PSD is intended for illustrative purposes, we derived equilibrium PSD from more complex PSD assumptions of TRMM PR 2A25 and GPM radar-radiometer combined retrievals (GPM 2A-CMB) spanning 1 March 2014 to 7 October 2014, roughly covering the period of overlap from the beginning of GPM observations until the end of TRMM PR data availability.

©2015. American Geophysical Union. All Rights Reserved.

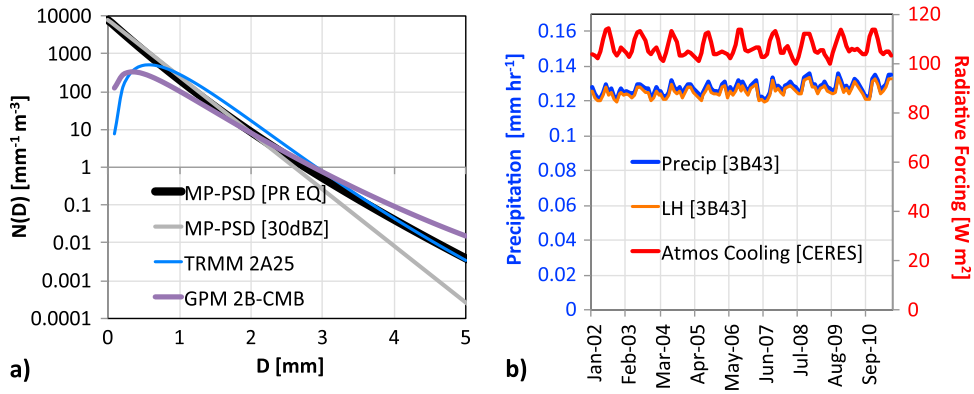

Figure 4. (a) Estimated tropics-averaged precipitation particle size distributions (PSD) from MP-PSD with 30 dB*Z* radar echo (MP-PSD [30 dB*Z*]), MP-PSD weighted with equilibrium PR echo frequencies (MP-PSD [PR EQ]), 10 month TRMM radar algorithm (TRMM 2A25), and 10 month GPM microwave-radar combined algorithm (GPM 2A-CMB). TRMM 2A25 and GPM 2B-CMB are averaged from 1 March 2014 to 7 October 2014. (b) Time series of monthly tropical mean precipitation from TRMM 3B43 (Precip [3B43]), estimated latent heat (LH) from 3B43 (LH [3B43]), and atmospheric radiative cooling rate estimated from Clouds and the Earth's Radiant Energy System (CERES) product (Amos Cooling [CERES]).

From 2A25, the Z and R values were collected from each profile at 1.5 km agl from all scan angles where the reflectivity was at least 20 dBZ. Following the PSD model used by 2A25 [*Iguchi et al.,* 2000], a gamma distribution ($N(D) = N_0 D^{\mu} \exp(-\lambda D)$) is assumed with dispersion parameter $\mu = 3$. Under this assumption, λ and N_0 can be determined from Z and R. The 2A25-derive equilibrium PSD in Figure 4a shows a reduction in particle number density for smaller particles due to the assumed dispersion parameters, while the PSD is quite similar for larger diameters (>3 mm) to those of the MP-PSD (Figure 4a). Although not shown here, month-to-month frequencies are nearly identical to the 10 month average, and also, the whole spectrum of PSD is depicted in Figure S1 in the supporting information.

While using a similar gamma distribution, GPM 2B-CMB estimates N_0 an ensemble Kalman filtering approach for inverting signals from Dual-Frequency Precipitation Radar (DPR) and GPM Microwave Imager (http://pps.gsfc.nasa.gov/atbd.html, *Grecu et al.* [2011]). Only observations within two scans of DPR nadir are used to derive 10 month climatology in order to avoid off-nadir clutter issue in the Ku-band echo. Figure 4a shows that the equilibrium PSD of GPM 2B-COMB is more broadly distributed than that from PR 2A25; i.e., more large-size particles and less small-size raindrops. TRMM PR 2A25 retrieval is optimized to maximize the consistency between Ku-band radar-retrieved and surface reference estimates of total path-integrated attenuation. GPM 2B-COMB retrieval is designed to incorporate additional information such Ka-band echo and high-frequency microwave brightness temperature. This could result in systematically different from single-frequency radar-only retrievals. In addition, the TRMM satellite orbit pattern (37° inclination orbit) could oversample subtropical shallow precipitation systems relative to GPM (65° inclination orbit), even when only GPM data from the tropical domain are considered.

The equilibrium PSDs of PR 2A25 and GPM 2B-COMB are formed closely to lognormal distributions, but the detailed distribution in the tail is more narrowly distributed than the actual lognormal PSD (not shown here). Overall, tropics-integrated PSDs are relatively different among the three estimates, and further investigation and algorithm improvement are required for better estimation of equilibrium precipitation PSD. In addition, this estimate does not include light precipitation below the PR and DPR detection limit.

If we add precipitation mass and terminal velocity in equation (4), total topical precipitation rate can be derived by integrating the entire particle flux distributions,

$$R|_{\text{tropics}} = \int \rho_l \frac{\pi}{6} D^3 \, V_t(D) \, N(D)|_{\text{tropics}} \mathrm{d}D. \tag{9}$$

If we assume the tropical microphysics to be in quasi-equilibrium state:

$$\frac{\partial N(D)|_{\text{tropics}}}{\partial t} \approx 0, \tag{10}$$

©2015. American Geophysical Union. All Rights Reserved.

we find simply nearly constant total precipitation:

$$R|_{\text{tropics}} \approx \text{const.} \tag{11}$$

Figure 4b shows the time series of monthly tropical mean precipitation rate (thick line) from the 3B43 product (monthly product of 3B42). The tropics mean precipitation rate is 0.127 mm h^{-1} with monthly standard deviation of 0.003 mm h^{-1} (~2.3% of deviation). This small variance satisfies equation (11), supporting the precipitation microphysics quasi-equilibrium hypothesis.

Further, the surface precipitation rate is directly associated with the atmospheric latent heat rate (LH), because the surface precipitation rate is equal to the net condensation rate of cloud particles:

$$\text{LH} = \frac{L_v}{C_p}\frac{M_{\text{cond}\ -\ \text{evap}}}{M_{\text{air}}} = \frac{L_v}{C_p}\frac{R}{M_{\text{air}}}, \tag{12}$$

where L_v is latent heat rate of condensation/vaporization (= 2.5 × 10^6 J kg^{-1}), C_p is specific heat at constant pressure, $M_{\text{cond}\ -\ \text{evap}}$ is net (condensation minus evaporation) condensation mass, and M_{air} is air mass.

This simple relation directly states that intensity distributions of atmospheric LH rate should be in the quasi-equilibrium state for time scales of a day (section 3), and total tropical LH also should be nearly time-invariant state, since total precipitation rate is nearly constant:

$$\text{LH}|_{\text{tropics}} = \frac{L_v}{C_p M_{\text{air}}} R|_{\text{tropics}} \approx \text{const.} \tag{13}$$

With dry air specific heat C_p (1004.67 J kg^{-1} K^{-1}) and also applying mean tropical surface pressure ($P_s|_{\text{tropics}}$ = 994 mbar) to estimate M_{air} (= 10132 kg m^{-2}), mean tropical LH become 0.752 K d^{-1} or equivalently 88.58 W m^{-2}. Note that we also assume that tropical air mass and pressure profile are in quasi-equilibrium state, too.

Figure 4b also shows the tropical atmospheric radiative cooling rate (red lines) derived from the monthly product of the Clouds and the Earth's Radiant Energy System (CERES) Energy Balanced And Filled TOA and surface product [*Loeb et al.,* 2005]. The primary axis (unit of mm h^{-1}) and the secondary axis (unit of W m^{-2}) are scaled identically through equation (13). The CERES-derived mean atmospheric cooling rate is 106.4 W m^{-2} with 10 W m^{-2} of seasonal fluctuation. Small but distinct seasonal peaks of cooling rate exist in June and January. The residual of heat balance (~17 W m^{-2}) can be explained by contributions from the sensible heat flux [*Stephens et al.,* 2012]. Thus, in the tropical domain, it is confirmed that the net atmospheric cooling is roughly balanced by the release of atmospheric LH by precipitation.

Since the radiative cooling process creates a vertical gradient of potential temperature and convective adjustment [*Manabe and Strickler*, 1964], it is physically feasible to consider the impact of seasonal variability of net radiative cooling on adjusting the net tropical precipitation rate. Spearman correlation coefficients (= 0.44) between monthly atmospheric radiative cooling rate and LH also suggest the radiation-precipitation coupling in tropics. Furthermore, the small biseasonal oscillations of atmospheric radiative cooling rate are coincident to the small biseasonal oscillations of shallow precipitation frequencies (Figure 1b). This could be a mutual interaction that maintains the tropical atmosphere through cloud-radiative feedback [*Stephens,* 2005]. More accurate precipitation estimates are required for further investigation.

To conclude, our MQE hypothesis does not conflict with the satellite observational record of nearly constant precipitation rate, which is closely balanced with atmospheric radiative cooling rate.

5. Macroscopic View of Tropical Convection and Microphysics

In this study, we treat convection and precipitation microphysics as a planetary-scale phenomenon despite its underlying random nature in local environments. When we (i) take monthly 6.6 million samples of total precipitation columns over the tropics in a month, (ii) combine the MP-PSD and histogram climatology of PR echo, and (iii) consider the PR sampling volume (1.96 × 10^{10} m^3: 5 km footprint size), we can roughly estimate that the total number of precipitation particles in monthly PR sampling would be close to 3.3 × 10^{20} near the surface level. This number changes to some degree through perturbing PSD assumptions as reviewed in section 3, but it does not change the order of magnitude.

©2015. American Geophysical Union. All Rights Reserved.

One interesting point is that the order of this huge sampling number is close to that of molecules in the unit cubic centimeter ($= 2.69 \times 10^{19}\,\mathrm{cm}^3$) at standard temperature and pressure. In this sample, the ensemble of molecular dynamics and kinetic energy is treated as a deterministic macroscopic phenomenon; namely, the thermodynamic laws or diffusion laws that govern the state of atmosphere. This suggests that some complex microphysics processes and cloud dynamics could be much more simply explained with extremely large samples, i.e., over the entire tropics under radiative-convective quasi-equilibrium environment, analogous to laws of diffusion or thermodynamics.

Finally, we briefly mention major open questions related to our preliminary results and MQE hypothesis:

1. *Do MQE and CQE happen at shorter time scale than a day?* The new Integrated Multi-satellitE Retrievals for GPM (IMERG) provides precipitation estimate a 10 km grid precipitation map with 30 min temporal resolution. Also, emerging global cloud-resolving models with explicit microphysics [*Grabowski,* 2003; *Satoh et al.,* 2008] will be a possible tool for studying MQE adjustment time.
2. *Why precipitation and LH intensity must be distributed in this shape?* The earliest study of *Bjerknes* [1938] provides a simple framework that explains physical reasoning of a small fraction of LH-driven buoyant updraft release versus a large fraction of sinking motion through radiative cooling. However, we need more robust analytic framework.
3. *What is the equilibrium precipitation size distribution*? The GPM 2B-CMB retrieval will continue to be refined and improved against the ground validation sites to constrain the assumptions of PSDs [*Williams et al.,* 2014]. It is also important to include W-band cloud-profiling radar for including light-precipitation microphysics [*Mitrescu et al.,* 2010].

While these new observational platforms and numerical tools will promise improved understanding of MQE, it also requires theoretical development, possibly introducing the microphysics theory into statistical mechanics, analogous to the theoretical establishment of thermodynamic laws. Finding of the robust microphysics laws would shed light on tropical meteorology as well as climate model parameterizations [*Emanuel,* 2007]. A more complete proof requires much greater effort, which is beyond the scope of this short article; however, progress is encouraged for the community.

Acknowledgments
Authors are funded by the NASA Precipitation Measuring Mission (PMM) grant. This paper is dedicated to Joanne Simpson, who was the first TRMM Project Scientist, a pioneer in tropical convection, and who inspired future generations of atmospheric scientists. The TRMM data used in this manuscript are archived and distributed by the Goddard Earth Sciences (GES) Data and Information Services Center (DISC) (http://disc.sci.gsfc.nasa.gov/). GPM data release and update will be available through Precipitation Measurement Missions (PMM) website (http://pmm.nasa.gov/).

The Editor thanks Gerald Mace and an anonymous reviewer for their assistance in evaluating this paper.

References

Arakawa, A., and W. H. Schubert (1974), Interaction of a cumulus cloud ensemble with the large-scale environment, part I, *J. Atmos. Sci.*, *31*, 674–701, doi:10.1175/1520-0469(1974)031<0674:IOACCE>2.0.CO;2.

Bjerknes, J. (1938), Saturated-adiabatic ascent of air through dry-adiabatically descending environment, *Q. J. R. Meteorol. Soc.*, *64*, 325–330.

Emanuel, K. (2007), Quasi-equilibrium dynamics of the tropical atmosphere, in *The Global Circulation of the Atmosphere*, edited by T. Schneider and A. H. Sobel, pp. 186–218, Princeton Univ. Press, Princeton, N. J.

Grabowski, W. W. (2003), Impact of cloud microphysics on convective–radiative quasi equilibrium revealed by cloud-resolving convection parameterization, *J. Clim.*, *16*, 3463–3475, doi:10.1175/1520-0442(2003)016<3463:IOCMOC>2.0.CO;2.

Grecu, M., L. Tian, W. S. Olson, and S. Tanelli (2011), A robust dual-frequency radar profiling algorithm, *J. Appl. Meteorol. Climatol.*, *50*, 1543–1557, doi:10.1175/2011JAMC2655.1.

Hou, Y. A., R. K. Kakar, S. Neeck, A. A. Azarbarzin, C. D. Kummerow, M. Kojima, R. Oki, K. Nakamura, and T. Iguchi (2014), The global precipitation measurement mission, *Bull. Am. Meteorol. Soc.*, *95*, 701–722, doi:10.1175/BAMS-D-13-00164.1.

Huffman, G. J., R. F. Adler, D. T. Bolvin, G. Gu, E. J. Nelkin, K. P. Bowman, Y. Hong, E. F. Stocker, and D. B. Wolff (2007), The TRMM multi-satellite precipitation analysis: Quasi-global, multi-year, combined-sensor precipitation estimates at fine scale, *J. Hydrometeorol.*, *8*(1), 38–55, doi:10.1175/JHM560.1.

Huffman, G. J., R. F. Adler, D. T. Bolvin, and E. J. Nelkin (2010), The TRMM Multi-satellite Precipitation Analysis (TMPA), in *Satellite Rainfall Applications for Surface Hydrology*, edited by F. Hossain and M. Gebremichael, chap. 1, pp. 3–22, Springer, New York.

Iguchi, T., T. Kozu, R. Meneghini, J. Awaka, and K. Okamoto (2000), Rain profiling algorithm for the TRMM precipitation radar, *J. Appl. Meteorol.*, *39*, 2038–2052, doi:10.1175/1520-0450(2001)040<2038:RPAFTT>2.0.CO;2.

Loeb, G. N., S. Kato, K. Loukachine, and N. Manalo-Smith (2005), Angular distribution models for top-of-atmosphere radiative flux estimation from the clouds and the Earth's radiant energy system instrument on the Terra satellite. Part I: Methodology, *J. Atmos. Oceanic Technol.*, *22*, 338–351, doi:10.1175/JTECH1712.1.

Manabe, S., and R. F. Strickler (1964), Thermal equilibrium of the atmosphere with a convective adjustment, *J. Atmos. Sci.*, *21*, 361–385, doi:10.1175/1520-0469(1964)021<0361:TEOTAW>2.0.CO;2.

Marshall, S. J., and W. M. K. Palmer (1948), The distribution of raindrops with size, *J. Meteorol.*, *5*, 165–166, doi:10.1175/1520-0469(1948)005<0165:TDORWS>2.0.CO;2.

Matsui, T., X. Zeng, W.-K. Tao, H. Masunaga, W. Olson, and S. Lang (2009), Evaluation of long-term cloud-resolving model simulations using satellite radiance observations and multifrequency satellite simulators, *J. Atmos. Oceanic Technol.*, *26*, 1261–1274, doi:10.1175/2008JTECHA1168.1.

Mitrescu, C., T. L'Ecuyer, J. Haynes, S. Miller, and J. Turk (2010), CloudSat precipitation profiling algorithm—Model description, *J. Appl. Meteorol. Climatol.*, *49*, 991–1003, doi:10.1175/2009JAMC2181.1.

Munchak, S. J., C. D. Kummerow, and G. Elsaesser (2012), Relationships between the raindrop size distribution and properties of the environment and clouds inferred from TRMM, *J. Clim.*, *25*, 2963–2978, doi:10.1175/JCLI-D-11-00274.1.

©2015. American Geophysical Union. All Rights Reserved.

Satoh, M., T. Matsuno, H. Tomita, H. Miura, T. Nasuno, and S. Iga (2008), Nonhydrostatic Icosahedral Atmospheric Model (NICAM) for global cloud resolving simulations, *J. Comput. Phys.*, *227*, 3486–3514, doi:10.1016/j.jcp.2007.02.006.

Schubert, W. H., J. J. Hack, P. L. Silva Dias, and S. R. Fulton (1980), Geostrophic adjustment in an axisymmetric vortex, *J. Atmos. Sci.*, *37*, 1464–1484, doi:10.1175/1520-0469(1980)037<1464:GAIAAV>2.0.CO;2.

Simpson, J., R. F. Adler, and G. R. North (1988), A proposed Tropical Rainfall Measuring Mission (TRMM) satellite, *Bull. Am. Meteorol. Soc.*, *69*, 278–295, doi:10.1175/1520-0477(1988)069<0278:APTRMM>2.0.CO;2.

Stephens, L. G. (2005), Cloud feedbacks in the climate system: A critical review, *J. Clim.*, *18*, 237–273, doi:10.1175/JCLI-3243.1.

Stephens, L. G., J. Li, M. Wild, C. A. Clayson, N. Loeb, S. Kato, T. L'Ecuyer, P. W. Stackhouse Jr., M. Lebsock, and T. Andrews (2012), An update on Earth's energy balance in light of the latest global observations, *Nat. Geosci.*, *5*, 691–696, doi:10.1038/ngeo1580.

Tao, W.-K., et al. (2006), Retrieval of latent heating from TRMM measurements, *Bull. Am. Meteorol. Soc.*, *87*, 1555–1572, doi:10.1175/BAMS-87-11-1555.

Uijlenhoet, R. (2001), Raindrop size distributions and radar reflectivity-rain rate relationships for radar hydrology, *Hydrol. Earth Syst. Sci.*, *5*(4), 615–627, doi:10.5194/hess-5-615-2001.

Williams, R. C., et al. (2014), Describing the shape of raindrop size distributions using uncorrelated raindrop mass spectrum parameters, *J. Appl. Meteorol. Climatol.*, *53*, 1282–1296, doi:10.1175/JAMC-D-13-076.1.

Yano, J.-I., and R. S. Plant (2012), Convective quasi-equilibrium, *Rev. Geophys.*, *50*, RG4004, doi:10.1029/2011RG000378.

Zipser, J. E. (2003), Some views on "hot towers" after 50 years of tropical field programs and two years of TRMM data, *Meteorol. Monogr.*, *29*, 49, doi:10.1175/0065-9401(2003)029<0049:CSVOHT>2.0.CO;2.

©2015. American Geophysical Union. All Rights Reserved.